CONTENT

Nastia Degiuli, Carlo Giorgio Grlj, Ivana Martić*

A numerical study on the nominal wake of the Japan Bulk Carrier

University of Zagreb, Faculty of Mechanical Engineering and Naval Architecture, Ivana Lučića 5, Zagreb, 10000, Croatia
*Corresponding author: nastia.degiuli@fsb.unizg.hr

Original scientific paper
Received: November 14, 2025
Accepted: January 9, 2026
https://doi.org/10.65776/ep.20.4.1

Abstract

A key element in propeller design is the accurate determination of the nominal wake. Therefore, in the present study the nominal wake of the Japan Bulk Carrier is determined numerically at model scale, and the numerical results are validated with the available experimental data. The numerical approach is based on the Reynolds Averaged Navier–Stokes (RANS) equations closed with the Shear Stress Transport k-ω (SSTKO) turbulence model. The governing equations are discretized using the Finite Volume Method (FVM) to obtain an algebraic system of equations. The nominal wake is evaluated through numerical simulations that account for the free surface effects. A verification study is performed to quantify the numerical uncertainty associated with the mesh resolution and time step using the Grid Convergence Index (GCI) method. The validation study consists of a comparison between the numerically obtained velocity components and the corresponding experimental measurements. The contour plots of the dimensionless velocity components indicate that the numerically predicted axial velocity is higher than the experimental values, whereas the tangential and radial components show good agreement with the experimental data. The circumferentially averaged dimensionless axial velocity predicted numerically show good agreement between 0.4R to 0.8R, while at radii from 0.8R to 1R, the numerical results overpredict the axial velocity. Finally, the integral values of the nominal wake are calculated, where the relative deviation between the numerical and experimental results is equal to -2.72 %.

Keywords: *CFD, EFD, nominal wake, Japan Bulk Carrier, resistance test*

1. Introduction

The nominal wake, measured at the propeller disc plane, represents one of the most critical aspects of propeller design. Its accurate determination is essential not only for defining the propeller blade section geometry and local pitch distribution but also for evaluating the efficiency of Energy Saving Devices (ESDs) [1]. Traditionally, full-scale nominal wake predictions rely on towing tank measurements conducted at the model scale. However, due to the limited number of validation studies, no firm conclusions can be drawn regarding the accuracy of different wake-scaling procedures. Pronounced scale effects are observed because the nominal wake is strongly influenced by viscous phenomena [2, 3]. These effects manifest as lower axial velocity values at the propeller disc plane in model-scale conditions compared to full scale [4].

Zhang et al. [5] investigated the nominal wake at both model and full scale using numerical simulations in oblique flow and reported a lower mean wake fraction in full-scale simulations. The authors attributed this difference to viscous effects, particularly the relatively thicker boundary layer at model scale. Similarly, Dogrul et al. [6] performed viscous flow simulations around the KCS and KVLCC2 hull forms at different scales and observed reduced axial velocities obtained for lower Reynolds numbers, further confirming the significant scale dependency of the nominal wake.

Conventionally, towing tank experiments are employed to determine the nominal wake at model scale. Since such measurements in the towing tank are expensive and time-consuming, Computational Fluid Dynamics (CFD) has become an attractive alternative for both model- and full-scale analyses. As demonstrated by Farkas et al. [4], performing full-scale CFD simulations eliminates the need for wake-scaling corrections prescribed by the International Towing Tank Conference (ITTC) and avoids the associated uncertainties. The authors emphasized that full-scale CFD simulations offer distinct advantages for stern-flow optimization and the validation of ESD performance.

The influence of surface conditions on propeller performance and wake characteristics has also been highlighted in recent studies. Farkas et al. [7] performed numerical simulations of the open water test to evaluate the effect of biofouling on propeller open water characteristics. The study led to a new performance prediction method for fouled surfaces. The authors pointed out that additional investigations are required to assess the influence of surface roughness and fouling on propellers operating in a ship's wake. Subsequently, Farkas et al. [8] investigated the influence of biofilm on the nominal wake and demonstrated that its presence can reduce the integral value of the nominal wake of a bulk carrier by up to 7 %.

Wang et al. [9] examined the influence of scale effects on the nominal wake of a 4000 TEU containership through CFD simulations. The authors compared Double Body Simulations (DBS), which neglect the free surface effects, with Free Surface Simulations (FSS) and found that the free surface has a negligible influence on the nominal wake. However, a distinct dependence of the mean axial wake fraction on the Reynolds number was observed, which prompted the authors to propose a new scaling method. Guo et al. [10] further examined the nominal wake for the case of the KCS by modifying the aft hull form to reproduce a full-scale like wake distribution. Their results, validated using particle image velocimetry, demonstrated that the modified hull configuration effectively minimized scale-induced discrepancies, and the authors proposed a new approach to mitigate scale effects in nominal wake prediction.

The aim of the present study is the numerical determination of the nominal wake of the Japan Bulk Carrier (JBC) and the validation of the obtained results with the available experimental data [11]. The FSS where conducted to include the effects of the free surface on the numerically obtained nominal wake. The rest of the paper is structured as follows: Section 2 describes the case study, outlines the mathematical background of the numerical simulations, and presents the experimental setup. Section 3 discusses the results of the verification and validation studies. Finally, Section 4 summarizes the main conclusions and outlines directions for future work.

2. Methods

2.1 Case study

The JBC is used as a case study in the numerical analysis of the nominal wake. The JBC is a capsize bulk carrier that has a bulbous bow and a transom stern. It was developed by the National Maritime Research Institute at the Yokohama National University and the Ship Building Research Centre of Japan for the purposes of the CFD workshop held in 2015 [12]. In Table 1, the main parameters can be seen, and the 3D model is shown in Figure 1. Figure 2 illustrates the location of the propeller plane, along with the global coordinate system. The coordinate system is defined with its origin at the intersection of the aft perpendicular and the waterplane. The x-axis points toward the bow, the z-axis is oriented upward, and the y-axis is directed toward the port side.

Main Parameter	Value
Scale λ	40.264
Length between perpendiculars L_{PP}, m	6.954
Length of waterline L_{WL}, m	7.078
Breadth B, m	1.118
Draught T, m	0.410
Displacement volume ∇, m^3	2.733

Table 1. JBC main parameters.

Fig. 1. Isometric and side views of the 3D model used in the numerical simulations.

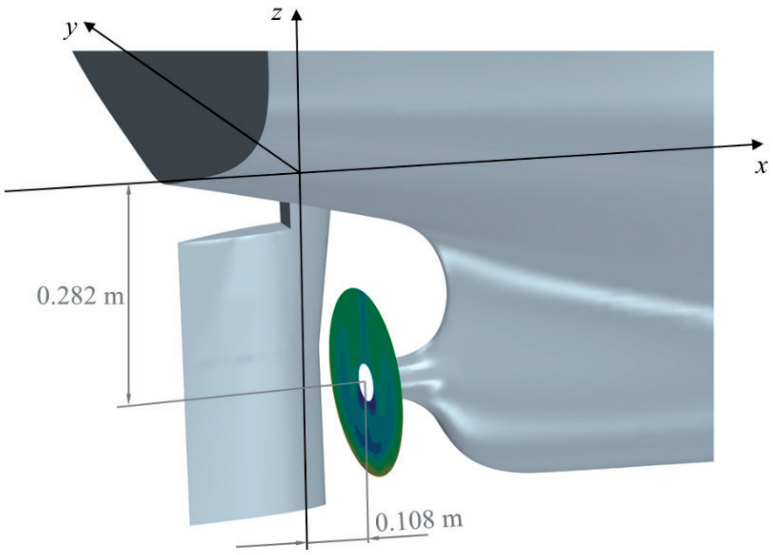

Fig. 2. Position of the propeller disc and the global coordinate system.

2.2 Experimental setup

The scale was selected to match the one used in the towing tank tests conducted at the Brodarski Institute in Zagreb [13]. As a part of the Croatian Science Foundation research project "Sustainable slow steaming for low carbon shipping", STARSHIP, an extensive experimental campaign was conducted including the resistance, open water and self-propulsion tests. The experimental campaign also included the measurements of the nominal wake. The nominal wake was obtained by measuring the absolute and static pressure using a five-hole Prandtl Pitot tube [11]. Figure 3 shows the installed five-hole Prandtl Pitot tube in the stern region, near the propeller.

Fig. 3. The five-hole Prandtl Pitot tube installed at the stern.

By subtracting the measured pressure values, the velocity components were calculated. The velocity components were obtained at radial positions equal to 0.35*R*, 0.55*R*, 0.74*R*, 0.94*R*, and 1.04*R* and at angular positions from 0° to 360° with 10° increments. According to long-term practice at the Brodarski Institute, the uncertainty associated with the measurements of absolute and static pressures at the propeller plane is within ±3 % [14].

2.3 Mathematical formulation

The numerical simulations are conducted with the commercial software STAR-CCM+ version 2306 [15] in which the mathematical model is based on Reynolds averaged Navier-Stokes (RANS) equations which read as follows:

$$\frac{\partial \overline{u}_i}{\partial x_i} = 0 \tag{1}$$

$$\rho \frac{\partial \overline{u}_i}{\partial t} + \rho \frac{\partial}{\partial x_j}(\overline{u}_i \overline{u}_j + \overline{u_i' u_j'}) = -\frac{\partial \overline{p}}{\partial x_i} + \frac{\overline{\tau}_{ij}}{\partial x_j} \tag{2}$$

where ρ is the fluid density, $\overline{u}_i$ is the averaged Cartesian component of the velocity vector, $\rho \overline{u_i' u_j'}$ is the Reynolds Stress Tensor (RST), $\overline{p}$ is the mean pressure, and $\overline{\tau}_{ij}$ is the mean viscous stress tensor.

For the closure of the governing equations, the two-equation Shear Stress Transport *k-ω* (SSTKO) turbulence model was used [14]. Within the SSTKO turbulence model two additional equations, one for the turbulent kinetic energy *k* and one for the specific dissipation *ω* are solved:

$$\frac{\partial}{\partial t}(\rho k) + \frac{\partial}{\partial x_i}(\rho k \overline{u}_i) = \frac{\partial^2 k}{\partial x_i^2}(\mu + \sigma_k \mu_t) + G_k + G_{nl} + \\ + G_b - \rho \beta^* f_{\beta^*}(\omega k - \omega_0 k_0) + S_k \tag{3}$$

$$\frac{\partial}{\partial t}(\rho \omega) + \frac{\partial}{\partial x_i}(\rho \omega \overline{u}_i) = \frac{\partial^2 \omega}{\partial x_i^2}(\mu + \sigma_\omega \mu_t) + G_\omega + D_\omega - \\ - \rho \beta f_\beta(\omega^2 - \omega_0^2) + S_\omega \tag{4}$$

where μ is the dynamic viscosity coefficient of the fluid, μ_t is the turbulent eddy viscosity, σ_k, σ_ω, β, and β^* are model coefficients, G_k, G_{nl}, G_b, and G_ω are the turbulent, non-linear, buoyancy, and specific dissipation production terms, respectively, f_{β^*} is the vortex-stretching modification factor, f_β is the free-shear modification factor, k_0 and ω_0 are the ambient values that counteract turbulence decay, and finally, S_k and S_ω are the user-specified source terms.

The governing differential equations were discretized using the Finite Volume Method (FVM). Since the numerical simulations accounted for the presence of a free surface, the interaction between the two immiscible fluids, i.e., water and air, was modelled using the Volume of Fluid (VOF) method. To ensure accurate resolution of the interface between the two phases, the High-Resolution Interface Capturing (HRIC) scheme was employed. Also, gravity is considered in the numerical simulations.

2.4 Numerical setup

In the present study, the numerical simulations that include the free surface effects are conducted, i.e., FSS. The numerical simulations are conducted at model scale to be able to validate the obtained results by directly comparing them to the experimental measurements. The computational domain in the FSS is generated according to the ITTC recommendations [16, 17]. In Figure 4 details of the computational domain are shown. The computational boundaries are placed at a distance large enough to prevent any undesired influence on the numerical solution. Velocity inlet is applied at the inlet, top and bottom boundaries, while outlet pressure is defined at the outlet boundary. At the side boundaries the symmetry boundary condition is used. For the hull and rudder surfaces, the no-slip wall boundary condition is applied. To avoid the wave reflections from the domain boundaries, the wave damping method [18] is applied at the inlet, outlet and side boundaries.

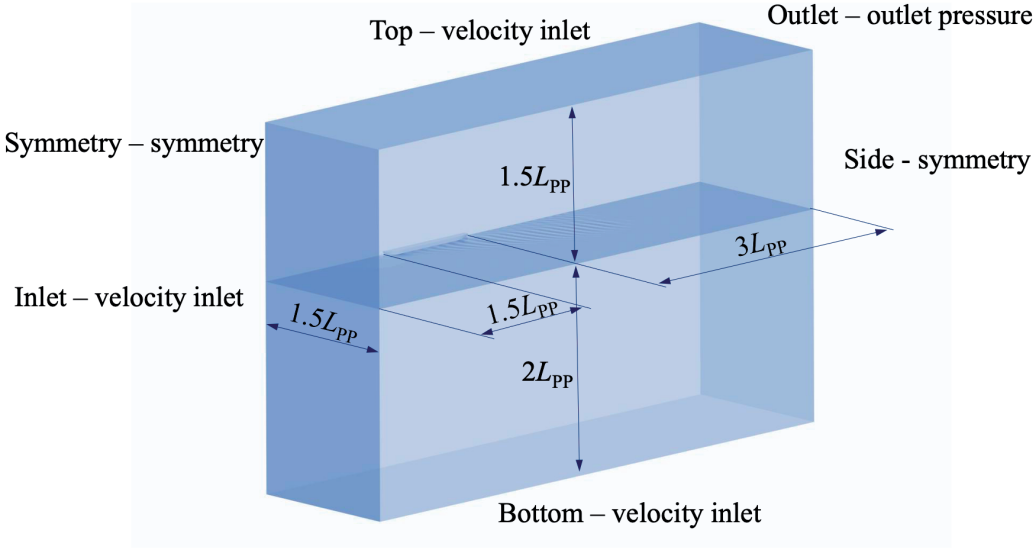

Fig. 4. Details of the computational domain.

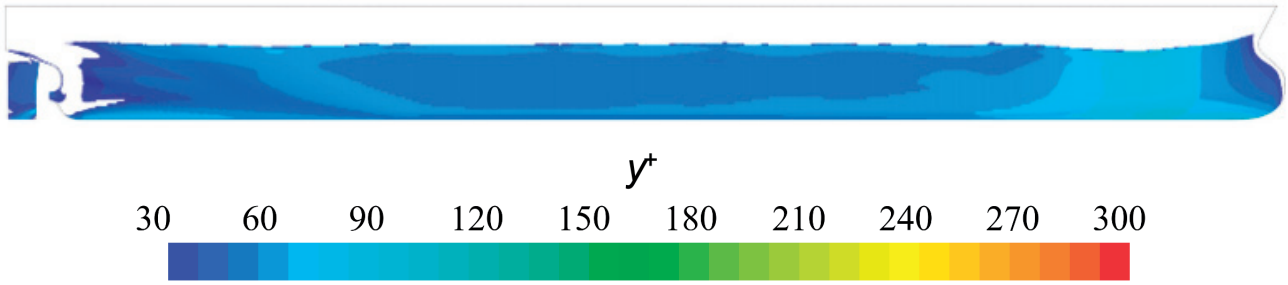

Fig. 5. Dimensionless wall distance y^+ obtained on the hull and rudder surfaces of the JBC.

The computational domain is discretized using unstructured hexahedral cells. The mesh is further refined in the following regions: free surface, Kelvin wake, bow, stern, and around the propeller disc.

The boundary layer is solved by applying wall functions and thus, the dimensionless wall distance y^+ is maintained above 30, as shown in Figure 5. The SSTKO turbulence model combined with wall functions was selected as a compromise between the computational resources needed to conduct the numerical simulations and the accuracy of the numerical results.

To maintain the y^+ value above 30, prism layers are generated in the vicinity of the hull and rudder surfaces. The distance between the centre of the first cell near the wall and the wall is carefully selected and additional prism layers are generated to keep a smooth transition to the rest of the mesh. Detailed views of the generated mesh with all applied refinements are presented in Figures 6 and 7.

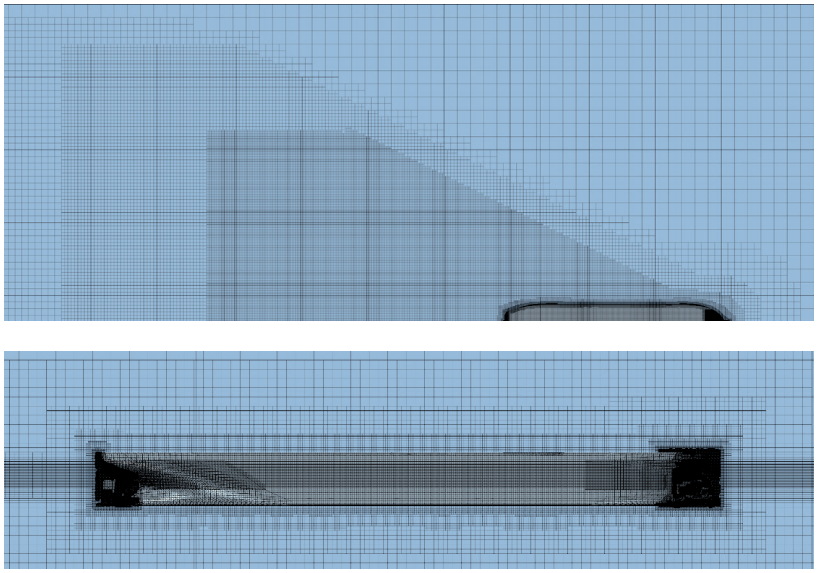

Fig. 6. The top and side views of the generated mesh.

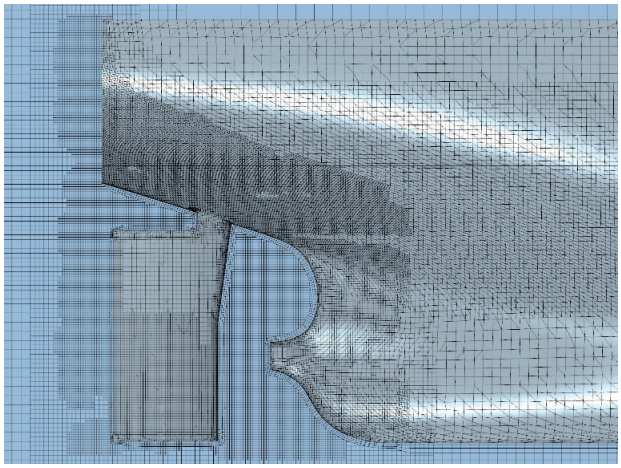

Fig. 7. Mesh details at the stern, near the propeller plane.

The numerical schemes used to solve the temporal, convection and gradient terms are selected following the recommendations given by Grlj et al. [19]. First-order discretization scheme is used for the temporal discretization, while second-order schemes are used for solving the convection and gradient terms.

The numerical simulations are carried out assuming smooth surfaces for both the hull and the rudder, and a fully developed turbulent flow throughout the computational domain. A freshwater density of 999.49 kg/m³ is used to replicate the conditions of the towing tank experiments, while the dynamic viscosity is set to 0.0012584 Pa·s. Since the towing tank measurements are performed at the design speed of the JBC, the inflow velocity in the numerical simulations is set to 1.176 m/s, which corresponds to a full-scale speed of 14.5 knots.

3. Results

3.1 Verification study

A verification study is conducted to assess the numerical uncertainty due to mesh resolution and time step. For the verification study, the Grid Convergence Index (GCI) method is used [20-22]. Three meshes are generated for the verification study, Table 2. The fine time step is defined as 0.125 % L_{PP}/v, while the medium and coarse time steps are obtained by multiplying the fine time step by 2 and 4, respectively.

Mesh	Number of cells N	Grid spacing h, m	Time step, s
Fine	3.5M	0.162	0.0074
Medium	1.7M	0.204	0.0148
Coarse	0.6M	0.282	0.0296

Table 2. Mesh sizes and time steps used in the verification study.

The verification study is conducted for the integral value of the nominal wake w_n. Table 3 shows the obtained results. The reported numerical uncertainty due to the mesh resolution is above 8 %. The reported order of method is close to 2, which indicates that the calculated *GCI* is reliable. The high numerical uncertainty can be attributed to the geometry of the JBC, which has a large block coefficient and exhibits strong flow recirculation in the stern region. Thus, the velocity distribution in the stern region varies a lot and to capture the local flow phenomenon fully, a more robust approach should be considered.

In contrast to the verification study for mesh resolution, the time step verification yielded better results, with the predicted *GCI* equal to 0.42 %. The observed order of method p, was considerably lower than the theoretical value of 2, indicating an overestimation of the computed numerical uncertainty. Consequently, the uncertainty associated with the time step can be considered negligible compared to that arising from the mesh resolution.

Parameter	Mesh resolution	Time step
ε_{21}	0.039	-0.002
ε_{32}	0.040	0.003
R	0.975	-0.570
p	2.196	0.820
ϕ_{ext}^{21}	0.600	0.646
e_{a}^{21}	0.061	0.003
e_{ext}^{21}	0.076	0.003
GCI_{fine}^{21}	8.83 %	0.42 %

Table 3. The verification study results.

3.2 Validation study

The numerical results presented in this subsection were obtained using the fine mesh and time step after the velocity components at the propeller plane had converged. The results presented in this subsection correspond to the final time step. Since the experimental velocity data below 0.4R were extrapolated, only values for higher radii are shown.

Figure 8 shows the comparison between the numerically and experimentally obtained distributions of the dimensionless axial velocity component at the propeller disc. The dimensionless axial velocity component predicted numerically is higher than the experimental values. A reason for this is the presence of rudder in the numerical simulations as opposed to the experimental setup. This is because the Prandtl Pitot tube was used in the towing tank and the installation of the required equipment occupied the stern area, specifically the rudder region. The hook like shape is visible in both cases, but the speed reductions obtained in the towing tank are greater compared to the speed reduction obtained numerically. In the region closer to the hub, the speed reductions predicted numerically are greater than those obtained experimentally.

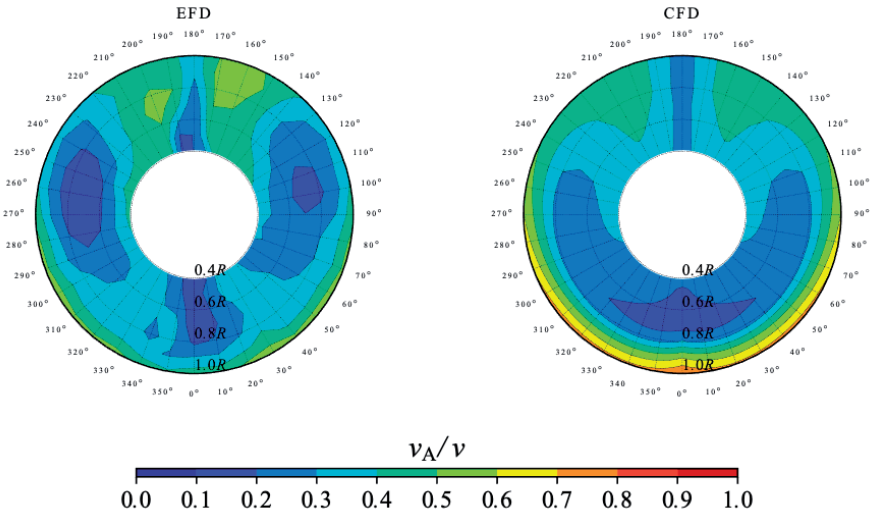

Fig. 8. Comparison between the numerical and experimental results of the dimensionless axial velocity component at the propeller disc.

A more detailed representation of the axial velocity component is shown in Figure 9, where the circumferential distributions of the dimensionless axial velocity for radii ranging from 0.4R to 1R are presented. The numerically predicted axial velocity between 0.4R and 0.8R show good agreement with the experimental data. At radii from 0.8R to 1R, however, the numerically obtained axial velocity becomes higher than the experimental values. There are larger speed reductions at circumferential position from 80° to 140° and likewise from 220° to 290° at radii from 0.6R to 0.8R. Also, at radii 0.6R and 0.7R larger discrepancies are evident from 0° to 60° and from 300° to 360°.

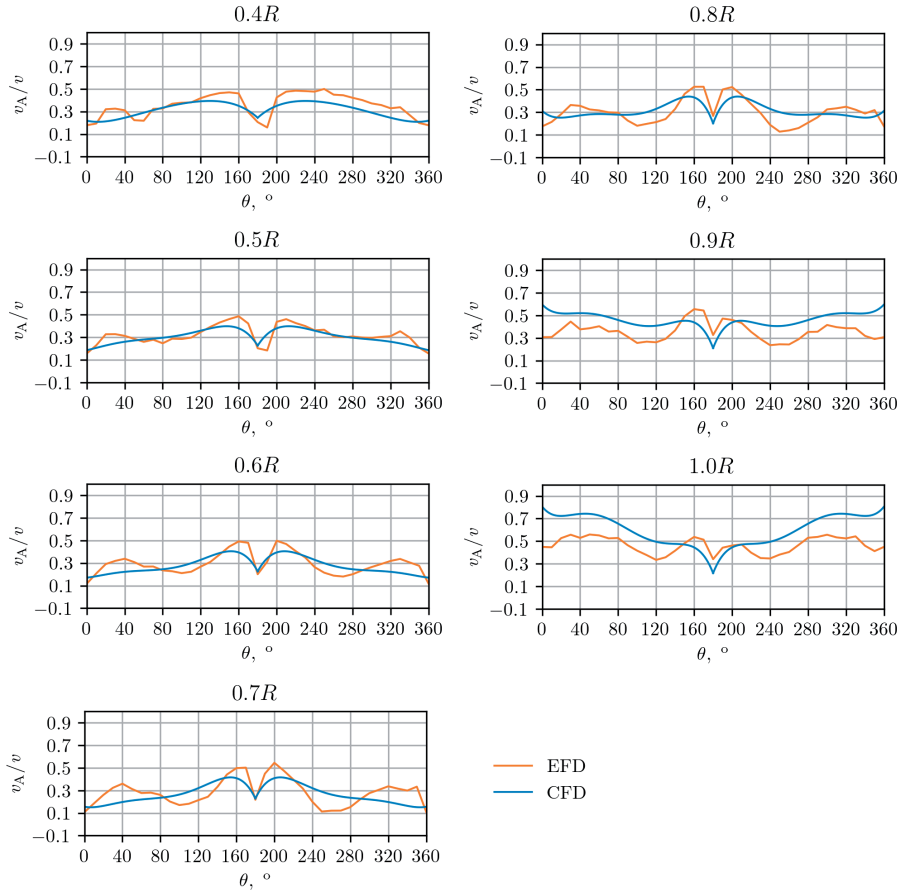

Fig. 9. The numerically and experimentally obtained circumferential distributions of the dimensionless axial velocity component at radii from 0.4R to 1R.

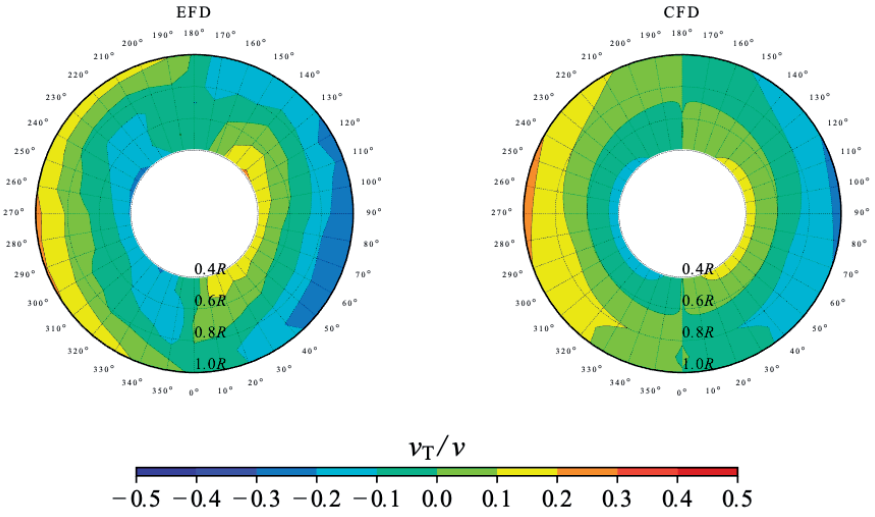

Fig. 10. Comparison between the numerical and experimental results of the dimensionless tangential velocity component at the propeller disc.

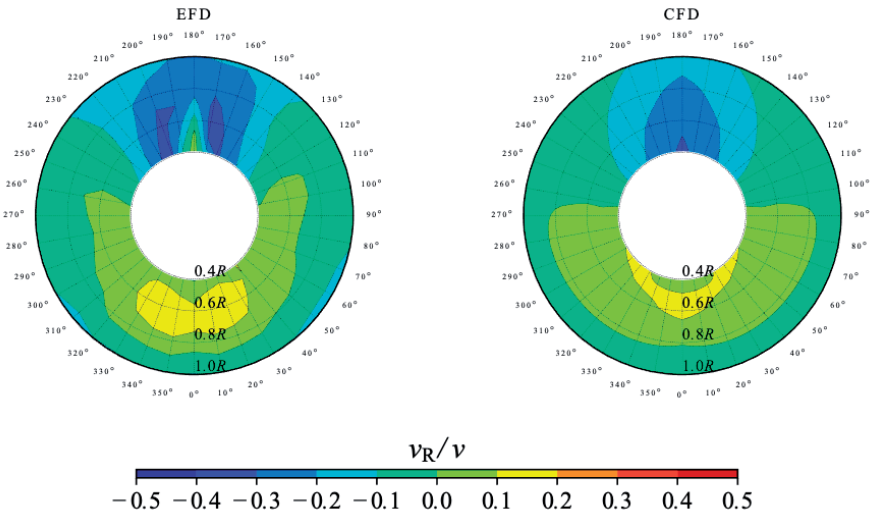

Fig. 11. Comparison between the numerical and experimental results of the dimensionless radial velocity component at the propeller disc.

Figures 10 and 11 show the comparisons of the tangential and radial velocity components obtained numerically and experimentally, respectively. Overall, the numerically predicted flow patterns agree well with the experimental observations. However, the experimental results exhibit a higher tangential velocity component in the region closer to the propeller hub compared to the numerical predictions. Similarly, in the region near the propeller tip, the tangential velocity measured in the towing tank is greater than that obtained from the numerical simulations. The towing tank measurements reveal an increase in the radial velocity component above the propeller hub that is not captured in the numerical simulations. Moreover, the experimental results show a more pronounced variation in the magnitude of the radial velocity component both above and below the hub compared to the numerical predictions.

Figure 12 presents the radial distribution of the circumferentially averaged dimensionless axial velocity component comparing the numerical and experimental results. Noticeable differences are observed between the numerical and experimental results in the range from 0.4R to 0.8R, while the discrepancies decrease with increasing radial position. At smaller radii, the numerically obtained axial velocity is lower than the experimental values, whereas between 0.9R and 1R it becomes slightly higher.

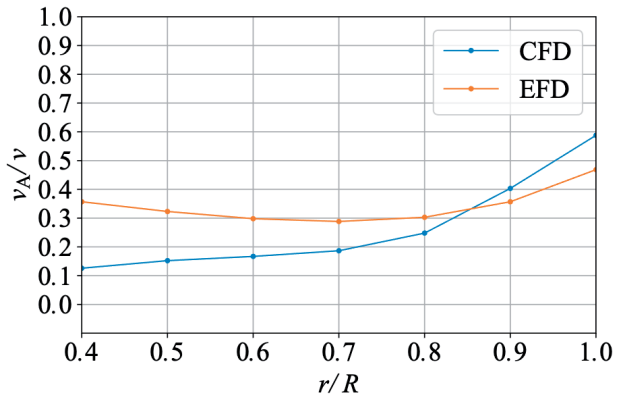

Fig. 12. Radial distribution of the circumferentially averaged dimensionless axial velocity component.

Finally, the integral value of the nominal wake is calculated as:

$$w_n = 1 - \frac{v_A}{v} \tag{5}$$

where v is the ship speed and v_A is the averaged axial velocity component over the propeller disc.

The numerically obtained integral value of the nominal wake is equal to 0.640, while the value derived from the experimental data is equal to 0.658. This corresponds to a relative deviation of only -2.72 %, indicating that despite local discrepancies in the axial velocity distribution, the overall nominal wake can be accurately predicted by the numerical simulations at model scale.

4. Conclusions

Numerical simulations of the resistance test were performed for the Japan Bulk Carrier at model scale, with particular emphasis on the flow characteristics in the propeller disc region. The presented results include contours of the dimensionless velocity components, axial, tangential, and radial, as well as the radial and circumferential distributions of the dimensionless axial velocity and the integral value of the nominal wake. A comprehensive verification study was carried out to quantify the numerical uncertainty associated with mesh resolution and time step. The findings revealed that mesh resolution had a major impact on the numerical uncertainty, while the influence of the time step was comparatively smaller. This can be attributed to the presence of recirculation zones in the stern region of the Japan Bulk Carrier, which caused fluctuations in the computed integral value of the nominal wake.

The validation study, based on the comparison of numerical and experimental results, showed that the numerically predicted dimensionless axial velocity component was generally higher than the experimental measurements, although the

characteristic hook like pattern was accurately reproduced. The contours of the tangential and radial velocity components also exhibited good agreement with the experimental data. The numerically obtained radial distribution of the circumferentially averaged axial velocity was lower than the experimental values between 0.4*R* and 0.8*R* but exceeded them at higher radii. Despite these local discrepancies, the relative deviation between the numerically and experimentally obtained integral values of the nominal wake was only -2.72 %, demonstrating that the overall wake characteristics were well captured by the numerical model.

5. Acknowledgement

This work was supported by the Croatian Science Foundation under the project number IP-2025-02-4779.

6. References

[1] Park, S., Oh, G., Rhee, S. H., Koo, B. Y., Lee, H. Full scale wake prediction of an energy saving device by using computational fluid dynamics. Ocean Eng. 101 (2015) 254-263.

[2] Regener, P., Mirsadraee, Y., Andersen, P. Nominal vs. effective wake fields and their influence on propeller cavitation performance. J. Mar. Sci. Technol. 6(2) (2018) 34.

[3] Ma, Z., Ji, N., Zeng, Q., Deng, X. and Shi, C. Influence of scale effect on flow field offset for ships in confined waters. Brodogradnja 75(1) (2024), 75106.

[4] Farkas, A., Degiuli, N., Martić, I., Dejhalla, R. Numerical and experimental assessment of nominal wake for a bulk carrier. J. Mar. Sci. Technol. 24 (2019), 1092-1104.

[5] Zhang, Y. X., Lai, M. Y., Ni, Y. G., Feng, L. CFD study of hull wakes in oblique flow at model and full scales. Appl. Ocean Res. 112 (2021) 102689.

[6] Dogrul, A., Song, S., Demirel, Y. K. Scale effect on ship resistance components and form factor. Ocean Eng. 209 (2020) 107428.

[7] Farkas, A., Degiuli, N., Martić, I. The impact of biofouling on the propeller performance. Ocean Eng. 219 (2021) 108376.

[8] Farkas, A., Degiuli, N., Martić, I. Impact of biofilm on the resistance characteristics and nominal wake. Proc. Inst. Mech. Eng. M: J. Eng. Marit. Environ. 234 (2020) 59-75.

[9] Wang, Z. Z., Xiong, Y., Wang, R., Shen, X. R., Zhong, C. H. Numerical study on scale effect of nominal wake of single screw ship. Ocean Eng. 104 (2015) 437-451.

[10] Guo, C., Wu, T., Zhang, Q., Luo, W., Su, Y. Numerical simulation and experimental studies on aft hull local parameterized non-GEOSIM deformation for correcting scale effects of nominal wake field. Brodogradnja 68(1) (2017) 77-96.

[11] Grlj, C.G., Degiuli, N., Martić, I. Scale effects on the resistance and propulsion characteristics of the Japan Bulk Carrier. Ocean Eng. 339 (2025), 122059.

[12] NMRI, 2015. Tokyo 2015 a workshop on CFD in ship hydrodynamics. https://t2015.nmri. go.jp/index.html

[13] Brodarski Institute. Report 6652-M. resistance, self-propulsion and 3D wake measurement test results Project: Japan Bulk Carrier - JBC. Brodarski Institute (2022).

[14] Grlj, C.G., Degiuli, N. and Martić, I. Experimental and numerical assessment of the effect of speed and loading conditions on the nominal wake of a containership. Brodogradnja 75(4) (2024), 75405.

[15] Siemens. STAR-CCM+ User Guide (2020).

[16] ITTC. Practical guidelines for RANS calculation of nominal wakes ITTC (2017).

[17] ITTC. Practical guidelines for ship CFD applications, 7.5-03-02-03. ITTC-Recommended Procedures and Guidelines (2011).

[18] Choi, J., Yoon, S. B. Numerical simulations using momentum source wave-maker applied to RANS equation model. Coast. Eng., 56 (2009) 1043-1060.

[19] Grlj, C. G., Degiuli, N., Martić, I. The impact of numerical parameters on the resistance characteristics of a container ship at the model and full scale. J. Mar. Sci. Eng. 11(9) (2023) 1672.

[20] Celik, I. B., Ghia, U., Roache, P. J., Freitas, C. J., Coleman, H., Raad, P.E. Procedure for estimation and reporting of uncertainty due to discretization in CFD applications. J. Fluids Eng. Trans. ASME. 130 (2008) 078001.

[21] Eça, L., Hoekstra, M. A procedure for the estimation of the numerical uncertainty of CFD calculations based on grid refinement studies. J. Comput. Phys. 262 (2014) 104-130.

[22] Mikulec, M., Piehl, H. Verification and validation of CFD simulations with full-scale ship speed/power trial data. Brodogradnja 74(1) (2023) 41-62.